EUROPEAN ORGANIZATION FOR NUCLEAR RESEARCH

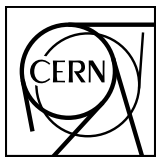

ALICE-PUBLIC-2022-013

Physics Preliminary Summary: Measurement of $\psi(2S)$ production as a function of charged-particle pseudorapidity density in pp collisions at $\sqrt{s} = 13$ TeV and p–Pb collisions at $\sqrt{s_{NN}} = 8.16$ TeV with ALICE at the LHC

ALICE Collaboration

Abstract

Charmonium production in pp collisions at center-of-mass energy of $\sqrt{s} = 13$ TeV and p–Pb collisions at center-of-mass energy per nucleon pair of $\sqrt{s_{NN}} = 8.16$ TeV is studied as a function of charged-particle pseudorapidity density with ALICE. Ground and excited charmonium states (J/ψ, $\psi(2S)$) are measured from their dimuon decays in the interval of rapidity in the center-of-mass frame $2.5 < y_{cms} < 4.0$ for pp collisions, and $2.03 < y_{cms} < 3.53$ and $-4.46 < y_{cms} < -2.96$ for p–Pb collisions. The charged-particle pseudorapidity density is measured around midrapidity ($|\eta| < 1.0$). In pp collisions, the measured charged-particle multiplicity extends to about six times the average value, while in p–Pb collisions at forward (backward) rapidity a multiplicity corresponding to about three (four) times the average is reached. The $\psi(2S)$ yield increases with the charged-particle pseudorapidity density. The ratio of $\psi(2S)$ over J/ψ yield does not show a significant multiplicity dependence in either colliding system, suggesting a similar behavior of J/ψ and $\psi(2S)$ yields with respect to charged-particle pseudorapidity density. The results are also compared with model calculations.

1 Introduction

Quarkonium production in hadronic collisions is a complex mechanism involving hard-scale processes, i.e., the creation of the quark–antiquark pair in the initial hard scattering, as well as the subsequent soft-scale process of the binding of the pair into a colorless final state [1]. The production mechanism is sensitive to the gluon content of the colliding hadrons and thus to the parton distributions of the incoming proton (PDF) or nucleus (nPDF) [2, 3]. In collisions involving heavy nuclei, modification to the production with respect to that in pp collisions may also arise from, e.g., energy loss that the heavy quarks experience while traversing the nucleus [4] or from subsequent interactions of the final states with comoving matter [5], both of which lead to a suppression of the quarkonium yield. Good understanding of these phenomena is imperative in order to correctly interpret the data from nucleus–nucleus collisions, where quarkonia are expected to be suppressed due to a deconfined partonic medium, i.e., the quark–gluon plasma (QGP) [6]. At the energies reached by the Large Hadron Collider (LHC), the suppression is partially compensated by a regeneration of the bound states in the medium [7].

Measurements of quarkonium production at the LHC in small collision systems, i.e., proton–proton (pp) and proton–nucleus (p–Pb) collisions, shed more light onto these processes. While measurements in pp collisions allow one to study the baseline production mechanisms of the quark–antiquark pair, the minimum-bias p–Pb data serve to probe the nuclear effects in conditions at which a formation of an extended QGP phase is not expected. In nuclear collisions, the initial-state nuclear effects impact the quark–antiquark pair created in the hard scattering. These effects manifest in the form of an enhancement and/or suppression of quarkonium production with respect to that in collisions of protons. Various initial-state effects are able to reproduce the measured nuclear modification of the J/ψ and $\Upsilon(1\mathrm{S})$ yields in p–Pb collisions at the LHC (see Refs. [8–13] and references therein). On the other hand, the excited charmonia ($\psi(2\mathrm{S})$) and bottomonia ($\Upsilon(2\mathrm{S})$, $\Upsilon(3\mathrm{S})$) display a suppression pattern different from that of their respective tighter bound states J/ψ and $\Upsilon(1\mathrm{S})$ [12, 14, 15]. Namely, the excited states were found to be more suppressed than the ground states. Such behavior cannot be explained with initial-state effects only and suggests that additional, final-state effects, which act on a bound quarkonium state, need to be considered. Furthermore, the nuclear effects have been found to depend on the multiplicity of particles produced in the p–Pb collision [16–19]. ALICE Collaboration has previously published a measurement, complementary to the one presented in hereby work, of J/ψ and $\psi(2\mathrm{S})$ production as a function of centrality in p–Pb collisions at $\sqrt{s_{\mathrm{NN}}} = 8.16$ TeV [19]. The study revealed that, except for the events in the lowest and highest event activity class, in which the nuclear modification between the two states is compatible, the $\psi(2\mathrm{S})$ yield is more suppressed than the J/ψ one. This result is consistent with the picture of the excited $\psi(2\mathrm{S})$ being more sensitive to final-state interactions.

Previous measurements of J/ψ production at forward rapidity as a function of multiplicity have revealed that the normalized yields increase linearly with the normalized charged-particle pseudorapidity density at midrapidity in pp collisions [20, 21] (both quantities being normalized to their corresponding averages in minimum-bias events), while for J/ψ production at midrapidity, the increase of the normalized yields has been found to be as stronger than linear [22]. In p–Pb collisions, the trend also depends on the J/ψ rapidity and hints at a deviation from a linear trend, suggesting slower- and stronger-than-linear increase for forward- and backward-rapidity J/ψ, respectively [18, 23]. The measured multiplicity-dependent behavior of hidden-charm hadrons is compatible with that of open-charm and beauty hadrons, suggesting a common origin of these phenomena independent of hadronization [24, 25].

Moreover, measurements in high-multiplicity pp and p–Pb collisions have revealed the presence of phenomena typically attributed to creation of QGP, e.g., long-range near- and away-side ridges in two-particle azimuthal correlations [26–29], collective motion of charged particles [30] and charmed hadrons [31–33]. Therefore, multiplicity-dependent studies in small systems provide a testing ground for examining the onset of QGP-like effects in collisions of energetic hadrons.

In this Note, measurements of inclusive $\psi(2S)$ production at forward rapidity as a function of charged-particle pseudorapidity density at midrapidity in pp and p–Pb collisions are presented. The inclusive yield contains a *prompt* component, which consists of states produced directly via hadronization of the quark–antiqaurk pair, and the *non-prompt* component originating from decays of *b*-hadrons. The $\psi(2S)$ is compared with the J/ψ state, by measuring the ratio of $\psi(2S)$ to J/ψ yields as a function of multiplicity. The data samples used in this study were collected with the ALICE detector at center-of-mass energies per nucleon pair of $\sqrt{s} = 13$ TeV for pp and $\sqrt{s_{\rm NN}} = 8.16$ TeV for p–Pb collisions.

2 Detector and data samples

The ALICE apparatus design and performance are documented in Refs. [34, 35]. The following section only describes those detector subsystems which are relevant for the present analyses.

The ALICE detector is instrumented at both central and forward rapidity. The ALICE forward muon spectrometer [36] detects muons in the pseudorapidity range $-4 < \eta < -2.5$ in the laboratory frame. It consists of five tracking stations (each of them consisting of two chambers of Cathode Pad Chamber detectors), followed by two triggering stations (two planes of Resistive Plate Chamber detectors each). A ten-interaction-length-thick absorber, made of carbon, concrete, and steel, is positioned in front of the tracking system to filter out most of the hadrons produced in the collisions. Remaining hadrons and low-momentum muons are absorbed by a second iron absorber positioned between the muon tracking chambers (MCH) and the muon trigger chambers (MTR). A 3 T·m dipole magnet, surrounding the third tracking station, provides the track bending for momentum evaluation. The Silicon Pixel Detector (SPD) is part of the ALICE central barrel [37]. It is used to reconstruct the primary vertex, reject events with collision pile-up, and estimate the charged-particle multiplicity of the collision. It corresponds to the two innermost layers of the Inner Tracking System (ITS) [37], which are positioned around the beam pipe and cover the pseudorapidity intervals $|\eta| < 2$ and $|\eta| < 1.4$, respectively.

The Minimum Bias (MB) trigger is provided by the V0 detector [38], two scintillator arrays covering the pseudorapidity ranges $2.8 < \eta < 5.1$ and $-3.7 < \eta < -1.7$. The timing information from the V0 is used to remove beam-induced background. Finally, the luminosity determination is obtained from the V0 information and, independently, using the T0 Cherenkov detectors [39], which cover $4.6 < \eta < 4.9$ and $-3.3 < \eta < -3.0$ [40, 41].

The pp data sample was collected at the center-of-mass energy of $\sqrt{s} = 13$ TeV between 2016 and 2018. Concerning the p–Pb sample, the hereby presented data were collected in 2016 at the center-of-mass energy per nucleon pair of $\sqrt{s_{\rm NN}} = 8.16$ TeV. In such asymmetric collisions, the nucleon–nucleon center-of-mass rapidity frame is shifted by $\Delta y = 0.465$ in the direction of the proton beam. The p–Pb data samples were recorded in two beam configurations: the *forward* configuration, in which the proton moves toward the spectrometer and quarkonia are measured in the proton-going direction, i.e. $2.03 < y_{\rm cms} < 3.53$; and the *backward* configuration, in which the proton moves away from the spectrometer and quarkonia are measured in the lead-going direction, i.e. $-4.46 < y_{\rm cms} < -2.96$. Events selected for these analyses were collected using a dimuon trigger which requires that two muons of opposite-sign charge are detected in the MTR in coincidence with the MB trigger, i.e., the detection of a signal in each side of the V0. The muons were required to have a transverse momentum $p_{\rm T}^{\rm trig}$, evaluated with the MTR, larger than about 0.5 GeV/c. In these data-taking periods, the maximum pile-up probability was about 0.5% for pp collisions, and about 4% for p–Pb collisions. Pile-up was further reduced to a negligible contribution by a dedicated event-selection strategy. An algorithm to tag events with multiple vertices reconstructed with the SPD was used for both collision systems. Additional selection criteria have been considered for p–Pb data, i.e., the correlation between the number of clusters in SPD and the number of track segments in SPD, the correlation between the signal amplitude in the V0 and the number of track segments in SPD, a timing criterion on the signal from V0, and the correlation of timing signals

from the two sides of the ZDC system. The integrated luminosity of the collected samples amounts to 24.38 ± 0.87 pb^{-1} in pp collisions and to 7.2 ± 0.2 nb^{-1} (10.6 ± 0.3 nb^{-1}) in forward (backward) p–Pb collisions.

3 Charged-particle multiplicity measurement

The number of track segments, *tracklets*, ($N_{\rm tracklet}$) formed by combining hits in both SPD [37] layers pointing to the primary vertex was used as the estimator of the charged-particle pseudorapidity density ($\mathrm{d}N_{\rm ch}/\mathrm{d}\eta$) at midrapidity. The information provided by the SPD was also used to compute the position of the primary vertex. In order to reduce the potential effects of the detector non-uniformities at its acceptance limits, the position of the primary vertex along the beam axis (z) was restricted to $|z_{\rm vtx}| < 10$ cm and only tracklets within the pseudorapidity range $|\eta| < 1$ were considered.

To account for the limited acceptance of the SPD and the variation of its conditions over time, a data-driven event-by-event correction [20, 22–24] was applied to the raw number of tracklets. The dependence of the SPD acceptance on the vertex position was corrected for by dividing the raw number of tracklets in each event by a $z_{\rm vtx}$-dependent renormalization factor, which was defined for each data-taking period as the average value of the $N_{\rm tracklet}$ distribution in the corresponding $z_{\rm vtx}$ interval, $\langle N_{\rm tracklet}\rangle(z_{\rm vtx})$, normalized to a reference value. The reference value was chosen as the maximum value of $\langle N_{\rm tracklet}\rangle$ over all $z_{\rm vtx}$ intervals and all data-taking periods. In order to account for event-by-event fluctuations, the renormalization factor was randomly smeared for each event using a Poisson distribution. Given the variations of the SPD conditions with time, the dataset was split into groups of sub-periods with a similar SPD status. In particular, for the three-year-long pp data-taking period, 12 groups were considered. The $\langle N_{\rm tracklet}\rangle(z_{\rm vtx})$ distributions were separately renormalized to the same reference value in each group. Once the correction was applied, events from all groups were merged and sorted into 9 intervals of corrected number of tracklets ($N^{\rm corr}_{\rm tracklet}$). Considering the smaller p–Pb data samples, 6 (8) $N^{\rm corr}_{\rm tracklet}$ intervals were defined for the forward (backward) p–Pb configuration in view of the $\psi(2S)$ signal extraction.

The estimation of $\mathrm{d}N_{\rm ch}/\mathrm{d}\eta$ from $N^{\rm corr}_{\rm tracklet}$ was performed using Monte Carlo (MC) simulations. DPMJET [42] and PYTHIA 8.2 [43] event generators were used to generate p–Pb and pp events respectively. In both cases, the transport of the generated particles through the detector was simulated using GEANT3 [44]. The correlation between the generated $\mathrm{d}N_{\rm ch}/\mathrm{d}\eta$ and the reconstructed $N^{\rm corr}_{\rm tracklet}$ was parameterized with a second order polynomial function. Other types of functional form were also tested to take into account potential deviations from the assumed second order polynomial function.

In the analysis of p–Pb collisions, these deviations from the assumed quadratic parameterization were taken as one source of systematic uncertainty, ranging from 0.3% at intermediate multiplicity to 4% in the lowest multiplicity interval. Another considered source of systematic uncertainty related to the MC sample was the uncertainty on the residual $z_{\rm vtx}$ dependence of $N^{\rm corr}_{\rm tracklet}$ originating from the differences between data and simulations, and the value of uncertainty was found to be close to 3%. In addition, events generated with EPOS-LHC [45] were also analyzed to evaluate the generator influence on the $\mathrm{d}N_{\rm ch}/\mathrm{d}\eta$ determination, resulting in a 2% systematic uncertainty in all multiplicity intervals. The process to determine the two latter sources of uncertainty is identical to the work described in Ref. [23]

In the case of pp collisions, all three potential contributions to systematic uncertainty, described in the previous paragraph, were evaluated together as a single contribution. As in the p–Pb case, EPOS-LHC was considered to account for possible dependence on the choice of the event generator. The overall systematic uncertainty on $\mathrm{d}N_{\rm ch}/\mathrm{d}\eta$ computed in each $N^{\rm corr}_{\rm tracklet}$ interval was found to range between 0.9% (at intermediate multiplicity) and 5% (lowest multiplicity interval).

Finally, the average charged-particle pseudorapidity density in the non-single diffractive (NSD) p–Pb collisions, $\langle \mathrm{d}N_{\rm ch}/\mathrm{d}\eta\rangle_{\rm NSD}$, was evaluated in an independent analysis. The measurement, whose value

Table 1: Summary of systematic uncertainties on the charged-particle pseudorapidity density measurements in $|\eta| < 1$ for pp collisions at $\sqrt{s} = 13$ TeV and p–Pb collisions at $\sqrt{s_{\rm NN}} = 8.16$ TeV.

	pp	p–Pb
$\mathrm{d}N_{\rm ch}/\mathrm{d}\eta$	0.9–5.3%	3.6–5.0%
$\langle \mathrm{d}N_{\rm ch}/\mathrm{d}\eta \rangle$	1.4%	4.1%

in a narrower pseudorapidity range can be found in Ref. [46], gives $\langle \mathrm{d}N_{\rm ch}/\mathrm{d}\eta \rangle_{\rm NSD} = 20.33 \pm 0.83$ (20.32 ± 0.83) for the forward (backward) configuration. The corresponding value for pp collisions was measured for inelastic events with at least one charged particle at midrapidity (INEL>0) and amounts to $\langle \mathrm{d}N_{\rm ch}/\mathrm{d}\eta \rangle_{\rm INEL>0} = 7.07^{+0.10}_{-0.08}$, computed from Ref. [47]. The total systematic uncertainties for both pp and p–Pb multiplicity measurements are reported in Table 1.

4 Charmonium yield determination

The normalized charmoniun yields were defined as the corrected yields in a given charged-particle pseudorapidity density interval i, $\mathrm{d}N^i/\mathrm{d}y$, divided by their multiplicity-integrated values , $\langle \mathrm{d}N/\mathrm{d}y \rangle$, according to

$$\frac{\mathrm{d}N^i/\mathrm{d}y}{\langle \mathrm{d}N/\mathrm{d}y \rangle} = \frac{N^i_{\psi(2S)}}{N_{\psi(2S)}} \frac{N^{\rm eq}_{\rm MB}}{N^{i,{\rm eq}}_{\rm MB}} \frac{(A\varepsilon)_{\psi(2S)}}{(A\varepsilon)^i_{\psi(2S)}} \frac{\varepsilon^i_{\rm MB}}{\varepsilon_{\rm MB}}\,, \tag{1}$$

where $N_{\psi(2S)}$ is the raw number of $\psi(2S)$ signals, $N^{\rm eq}_{\rm MB}$ is the number of equivalent minimum-bias (MB) events (defined later in this section), $A\varepsilon_{\psi(2S)}$ is the average acceptance-times-reconstruction efficiency for $\psi(2S)$, and $\varepsilon_{\rm MB}$ is the event-selection efficiency.

J/ψ and $\psi(2S)$ candidates were reconstructed by forming pairs of opposite-sign-charge muon tracks and computing their invariant mass. Muons were identified by requiring that each track candidate in the MCH matches with a track segment in the MTR. In addition, tracks were required to be reconstructed within $-4.0 < \eta^\mu < -2.5$, with their radial distance from the beam axis at the end of the front absorber being limited within $17.6 < R_{\rm abs} < 89.5$ cm, to ensure that only the tracks within detector acceptance were selected for further analysis.

Raw charmonium yields were extracted by fitting the invariant-mass distribution with a superposition of J/ψ and $\psi(2S)$ signal functions and a background function. Different combinations of functional forms were used to determine the raw yields and their uncertainties. The J/ψ and $\psi(2S)$ signal peaks were parametrized either with a Crystal Ball (CB) function or a pseudo-Gaussian function with power-law tails (as implemented first by the NA60 Collaboration) [48, 49]. The two functions differ in their parametrization including a Gaussian core and two asymmetric exponential tails. The J/ψ mass, width, and normalization were left free in the fit procedure, while the $\psi(2S)$ function parameters, apart from the normalization, were bound to those of J/ψ as explained in Ref. [50]. The $\psi(2S)$ mass was constrained by requiring that the difference with respect to the J/ψ mass was the one reported by the Particle Data Group in Ref. [51]. The $\psi(2S)$ width was taken as proportional to the J/ψ width. The ratio of $\psi(2S)$ and J/ψ peak widths was determined from Monte Carlo or data, as explained in Ref. [52], combining the values obtained with these two alternative options to define the raw charmonium yields. Tail parameters were obtained from data or Monte Carlo and fixed in the fits. In both the pp and p–Pb analyses, the tail parameters extracted from the respective multiplicity-integrated data and MC samples were used in the fit with CB signal function. For the NA60 function, the tail parametrization could only be extracted from MC for both collision systems. Additionally, the tails extracted from pp data and MC were also considered in the p–Pb analysis as well as those used in analysis described in Ref. [8]. The use of pp tails in p–Pb analysis was motivated by the better determination of the tails in the larger pp data sample, given the similar experimental conditions for these data-taking periods. To summarize, in the analysis of pp collisions, two sets of tail parameters were used in the fit of the CB function and one in the fit with the

NA60 function. In the p–Pb analysis, a total of five parametrizations of the CB tails and one of the NA60 tails were considered. Different functional forms were considered to describe the combinatorial background. For pp collisions, either a sum of two exponentials or a pseudo-Gaussian function whose width varies linearly with the invariant mass were used. Whereas for p–Pb collisions, the functions considered were either the product of an exponential and a fourth-order polynomial, or the sum of two exponential functions. The invariant-mass distribution was fitted multiple times per each multiplicity interval, each iteration varying the parametrizations of the signal and background components and varying the fit range. The number of candidates and their statistical uncertainties were evaluated from the average of the values over all trials, while their standard deviation was used to determine the systematic uncertainty. When computing the normalized charmonium yields or the normalized excited-to-ground state ratio, the systematic uncertainty due to the signal parametrization was considered as correlated across charged-particle multiplicity intervals, while the one due to the background description in the fit was treated as uncorrelated.

The equivalent number of MB events, $N_{\rm MB}^{\rm eq}$, was obtained from the number of dimuon-triggered events, $N_{\mu^+\mu^-}$, as $N_{\rm MB}^{\rm eq} = F_{\rm norm} \times N_{\mu^+\mu^-}$, where the normalization factor $F_{\rm norm}$ represents the probability of a dimuon trigger to occur in a MB-triggered event. $F_{\rm norm}$ was evaluated either by computing the probability of a coincidence of these two triggers in data or by exploiting an intermediate single-muon trigger [46].

The acceptance-times-efficiency $A\varepsilon$ of charmonia was determined via simulations with the PYTHIA 6 event generator coupled with GEANT3 to transport the particles through the detector. The simulations take into account the variation of the experimental conditions with time. As can be derived from Eq.1, the normalized yield is only sensitive to the variation of $A\varepsilon$ with charged-particle multiplicity. No variation of the $A\varepsilon$ due to the detector occupancy was observed. However, it is sensitive to the possible variation of the y and $p_{\rm T}$ distributions with multiplicity. The J/ψ analyses have shown a variation of $\langle p_{\rm T} \rangle$ with charged-particle multiplicity [22, 23]. Therefore, the influence of the MC input y and $p_{\rm T}$ distributions was studied. The exercise was done using an iterative procedure to describe the data for each multiplicity interval. Due to the limited size of the ψ(2S) signal, the procedure was performed for J/ψ. Three iterations were sufficient to converge, as verified by comparing the simulated $p_{\rm T}$ and y distributions to those obtained from data and corrected for $A\varepsilon$. For pp data, a 4% variation of $A\varepsilon$ was found from the lowest to the highest multiplicity interval, and used to correct the normalized yield measurement. No dependence of $A\varepsilon$ with charged-particle multiplicity was observed for p–Pb collisions, therefore no correction was applied. The different behavior of $A\varepsilon$ with charged-particle multiplicity in pp and p–Pb collisions is understood as a consequence of the higher $\langle p_{\rm T} \rangle$ values in pp collisions at $\sqrt{s} = 13$ TeV [52], and the steep increase of the acceptance-times-efficiency with $p_{\rm T}$ above 3 GeV/c.

The extracted yields needed to be corrected for the efficiency of the MB trigger to select the INEL>0 (NSD) events, $\varepsilon_{\rm INEL>0}$ ($\varepsilon_{\rm NSD}$). The $\varepsilon_{\rm INEL>0(NSD)}$ was evaluated for each multiplicity interval and found to be equal to unity in all the intervals apart from the one with the least event activity. A 1% correction was determined and applied to the first multiplicity interval.

The following sources of systematic uncertainty on normalized ψ(2S) yields were considered: (i) the signal extraction, (ii) the normalization factor, (iii) the event-by-event $N_{\rm tracklet}$ to $N_{\rm tracklet}^{\rm corr}$ correction, (iv) effects of the resolution and of the pile-up on the multiplicity classification, and (v) the event-selection efficiency. Except for the correlated uncertainty on event-selection efficiency and the partly correlated uncertainty on signal extraction, all sources of systematic uncertainty have been considered as uncorrelated in multiplicity. The systematic uncertainties on the charmonium yields in each multiplicity interval, normalized to their multiplicity-integrated values, were determined directly for the ratios. Likewise, the uncertainties on the normalized excited-to-ground state ratios were determined for the ratio directly rather than propagated from individual state yields. The details on the signal extraction have been explained previously in this section. The central values were determined averaging the results of the fits by varying the signal and background functions, as well as the invariant-mass fit interval. The systematic uncertainty

Table 2: Sources of systematic uncertainty on the normalized $\psi(2S)$ yields. The values marked with asterisk (diamond) are (partly) correlated in multiplicity.

Source	pp	p–Pb	
	$2.5 < y_{\rm cms} < 4.0$	$2.03 < y_{\rm cms} < 3.53$	$-4.46 < y_{\rm cms} < -2.96$
Signal extraction	4–5% $\diamond$	4–8% $\diamond$	5–13% $\diamond$
Event-by-event $N_{\rm tracklet}^{\rm corr}$	1–2%	2%	2%
Resolution and pile-up	–	2%	2%
Event-class normalization	1%*	1%*	1%*

was evaluated as the standard deviation between the values for all individual trials, ranging from 4% to 5% for pp data, and 4% to 8% (5% to 13%) for p–Pb data at forward (backward) rapidity. The influence of the normalization factor was evaluated by computing $F_{\rm norm}$ with different methods and studying its variation with time (see Ref. [23]). The effect on the result was found to be negligible in the measured multiplicity intervals. The impact of the chosen method for the event-by-event $N_{\rm tracklet}$ to $N_{\rm tracklet}^{\rm corr}$ correction was studied in Refs. [20, 23, 24]. Both the reference value used to scale the $N_{\rm tracklet}$ distribution as well as the randomization function considered to introduce a Poissonian fluctuation of the values were varied. The influence of these variations on the normalized yields ranges around 1–2% (2%) for pp (p–Pb) collisions. The influence of the resolution on the multiplicity axis and the possible remaining pile-up were evaluated as a single contribution by repeating the analysis multiple times by varying the pile-up rejection criteria or introducing a small shift of the $N_{\rm tracklet}^{\rm corr}$ intervals. The estimated uncertainty amounts to 2% in p–Pb results and was found to be negligible for pp data. The uncertainty on event-class normalization, originating from the INEL>0 or NSD event-selection efficiency, was evaluated as in Ref. [46]. A 1% uncertainty was assigned to both pp and p–Pb measurements, correlated in multiplicity. The contributions to the systematic uncertainty of the normalized $\psi(2S)$ yields are summarized in Table 2.

The same sources of systematic uncertainty were studied for the normalized $\psi(2S)$-over-J$/\psi$ ratios. In this case, the influence of the event-by-event $N_{\rm tracklet}^{\rm corr}$ correction, as well as that of the resolution and pile-up were found to be negligible. The uncertainty originating from the normalization to the INEL>0 (NSD) event class in pp (p–Pb) collisions cancels out in the ratio. Signal extraction is the sole contributor to the systematic uncertainty on the normalized $\psi(2S)$-over-J$/\psi$ ratio, and amounts to 4–5% for pp results, and to 4–8% (5–12%) for forward (backward) rapidity p–Pb measurements.

5 Results

In pp collisions, the measured charged-particle multiplicity spans up to about six times the average value. In p–Pb collisions at forward (backward) rapidity, the yields have been measured up to about three (four) times the average multiplicity. The normalized $\psi(2S)$ yield increases with increasing multiplicity, presenting a similar trend in pp collisions at $\sqrt{s} = 13$ TeV and p–Pb collisions at $\sqrt{s_{\rm NN}} = 8.16$ TeV. The p–Pb results at forward and backward rapidity are compatible between each other within uncertainties.

The ratio of normalized $\psi(2S)$-over-J$/\psi$ yields is evaluated to outline possible differences between multiplicity dependence of the production of the excited $\psi(2S)$ and ground-state J$/\psi$ with reduced uncertainties. The double ratios, obtained by dividing the $\psi(2S)$-over-J$/\psi$ yield ratios in multiplicity intervals by the multiplicity-integrated ratios, are shown in Fig. 2. The measurements are compatible with unity within uncertainties for both colliding systems. The double ratio in pp collisions, which is more precise than that in p–Pb, is consistent with a linear trend, either with a null (χ^2/ndf = 2.1) or a negative slope (χ^2/ndf = 1.5, free value of slope -0.05 ± 0.02). The measurements are compared with theoretical calculations in Fig. 3, 4, and 5.

The results from the PYTHIA 8.2 event generator [43] for pp collisions at $\sqrt{s} = 13$ TeV are shown

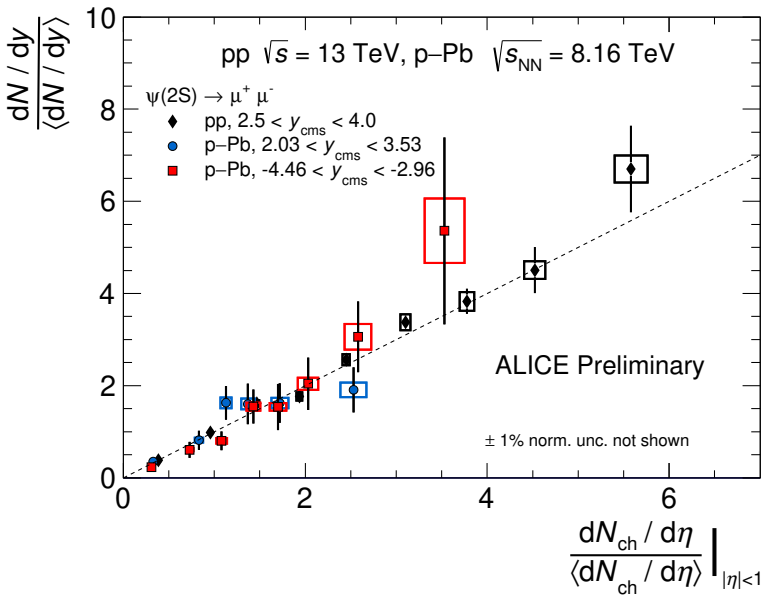

Fig. 1: The normalized $\psi(2S)$ yield as a function of the normalized charged-particle pseudorapidity density in pp collisions at $\sqrt{s}$ = 13 TeV and p–Pb collisions at $\sqrt{s_{NN}}$ = 8.16 TeV. Quoted is the correlated event-class normalization uncertainty. The pp results are normalized to the INEL>0 event class, whereas the p–Pb ones refer to the NSD one.

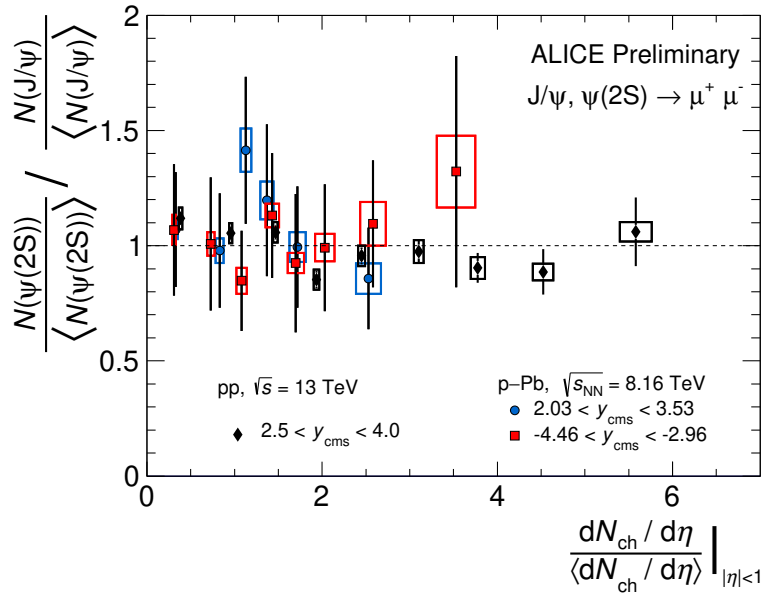

Fig. 2: Ratio of normalized $\psi(2S)$-over-J/ψ yield as a function of the normalized charged-particle pseudorapidity density in pp collisions at $\sqrt{s}$ = 13 TeV and p–Pb collisions at $\sqrt{s_{NN}}$ = 8.16 TeV. The pp results are normalized to the INEL>0 event class, whereas the p–Pb ones refer to the NSD one.

in Fig.3. In contrast to PYTHIA 6, PYTHIA 8.2 allows charm and beauty quarks to be involved in secondary hard processes, i.e., in multiparton interactions (MPI). From the implementation of the MPI mechanism a simple scaling is expected, in which the multiplicity of charged particles is proportional to the number of MPI and to the amount of hard processes taking place in a collision. At first order, this results in an increasing trend of the normalized quarkonium yields as a function of the normalized charged-particle multiplicity, with a slope close to unity. The $\psi(2S)$ yield measurement is described within uncertainties by the PYTHIA 8.2 event generator, both with and without the color-reconnection (CR) contribution. No significant difference is observed between the two configurations of PYTHIA 8.2, even though the naive expectation is that of a steeper trend in the simulation with CR, caused by the effective reduction of the charged-particle multiplicity at large multiplicities in the CR scenario. A tension appears on the comparison of the measurement and the calculation of the $\psi(2S)$-over-J$/\psi$ ratio as a function of the charged-particle multiplicity, as can be seen in Fig.3(b). For values of normalized charged-particle multiplicity below unity, the simulations yield values of the $\psi(2S)$-over-J$/\psi$ ratio lower than unity, while the measured values in the same multiplicity range reach above unity. A different event activity bias could be the explanation for the discrepancy found at low multiplicity. For instance, in PYTHIA 8.2, events with $\psi(2S)$ are, on average, biased towards a larger event activity as a consequence of its larger mass. This interpretation can not be confirmed, nor refuted, with the current measurement precision.

High-energy hadronic collisions can also be simulated in the percolation framework [53]. This Note shows calculations from this model only for p–Pb collisions. The key ingredient of this model are the color ropes or flux tubes (strings), that are formed in each parton–parton interaction and constitute the main source of particle production. The strings have non-negligible transverse size and can interact among each other. In particular, they can overlap, reducing their effective number and, consequently, the particle production. In this string model [54], the number of quarkonia is assumed to be proportional to the number of partonic scatterings, which corresponds to the number of produced strings. Instead, the charged-particle multiplicity scales with the number of participants due to the influence of shadowing [55], parton saturation [56], or percolation [53]. For p–Pb collisions, the percolation calculations shown in this Note are coupled to the comover model [5, 57] and to EPS09 nPDFs [58], the latter having been added to account for nuclear effects. In the comover model [5, 57], quarkonia can be dissociated by interacting with the surrounding comoving particles in the final state. The probability for this to happen depends on the binding energy of each quarkonium state and on the density of comoving particles. The latter determines the uncertainties of the model. The rapidity distribution of the density of hadrons is parametrized taking into account the geometry of the collision [59]. The EPS09 uncertainties have a sizable influence on the model estimate of the yields but cancel in the $\psi(2S)$-over-J$/\psi$ ratio. Feed-down contributions from decays of other charmonium states are taken into account in the calculation. The normalized $\psi(2S)$ yields in p–Pb collisions are described within uncertainties by the percolation + comover + EPS09 calculation (see Fig.4(a) and 5(a)). The model expects a nearly linear increase of the yield at backward rapidity, compatible with the measured one. The model calculation at forward rapidity also describes the measurement, within the large EPS09 uncertainties. It is to be noted that the measured values are on the upper edge of the uncertainty band of the prediction.

In the comover scenario [5, 57], the probability of $\psi(2S)$ to dissociate due to interactions in the final state is larger than that of J$/\psi$ due to its lower binding energy. The effect increases with charged-particle multiplicity, i.e., with the comover density. This results in a decreasing trend of the double ratio with increasing charged-particle multiplicity, in contrast to PYTHIA 8.2 simulations for pp collisions, which do not include final-state effects. The uncertainties shown in the comover calculation for the double ratio in pp collisions represent the influence of varying by 15% the density of comoving particles. The double ratios for pp collisions are described by the comover calculation within uncertainties, see Fig.3(b). The data-to-model comparison suggests a steeper decrease in the model calculation than in the measured data points, albeit no firm conclusion can be drawn with the current precision of the measurement. The double

ratios measured in p–Pb collisions are shown in Figs. 4(b) and 5(b). The measurements, while weighted by a large uncertainty, are consistent with the comover calculation, which predicts a stronger suppression of the excited states at backward rapidity. Previous studies of the relative suppression between the two charmonium states indeed revealed a stronger suppression at backward rapidity, largely independent of multiplicity [16, 19].

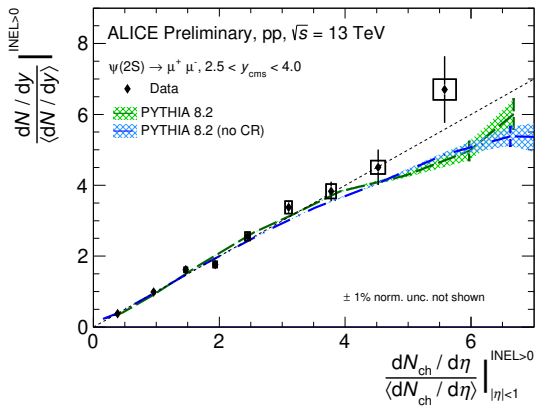

(a) Normalized ψ(2S) yield

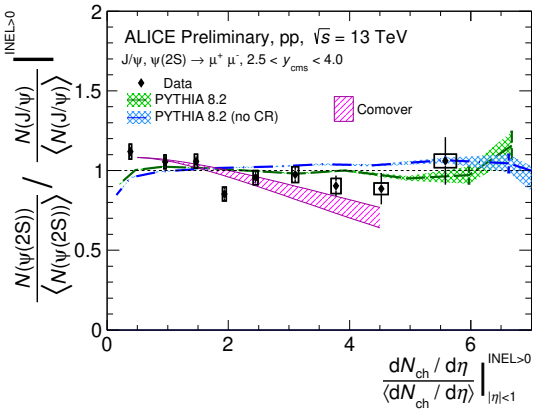

(b) Normalized ratio of ψ(2S) over J/ψ

Fig. 3: The normalized ψ(2S) yield and the ratio of normalized ψ(2S)-over-J/ψ yields at $2.5 < y_{\rm cms} < 4.0$ as a function of the normalized charged-particle pseudorapidity density in pp collisions at $\sqrt{s} = 13$ TeV. Measurements are compared with the following models: PYTHIA 8.2 [43], PYTHIA 8.2 without color reconnection (no CR) [43], comovers [5]. Quoted is the correlated event-class normalization uncertainty.

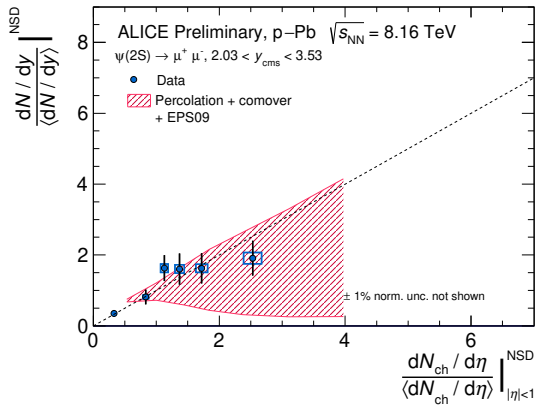

(a) Normalized ψ(2S) yield

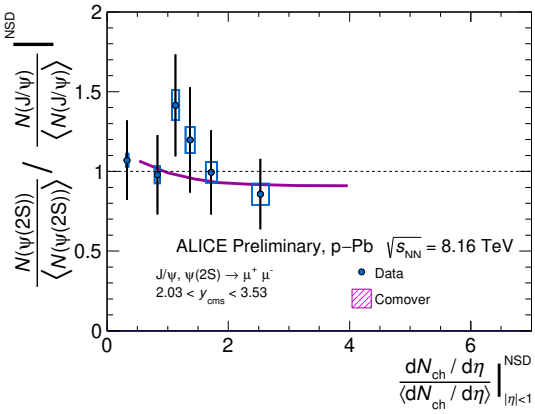

(b) Normalized ratio of ψ(2S) over J/ψ

Fig. 4: The normalized ψ(2S) yield and the ratio of normalized ψ(2S)-over-J/ψ yields at $2.03 < y_{\rm cms} < 3.53$ as a function of the normalized charged-particle pseudorapidity density in p–Pb collisions at $\sqrt{s_{\rm NN}} = 8.16$ TeV. Measurements are compared with the percolation calculation [53] coupled with comover model [5] and EPS09 nPDF [58]. Quoted is the correlated event-class normalization uncertainty.

To better contextualize the results presented in this Note, one needs to consider previously published results on multiplicity-dependent quarkonium production. The normalized yields of charmonium and bottomonium ground and excited states at large rapidity increase with the normalized charged-particle multiplicity at midrapidity with a similar approximately linear trend (with gradient equal to unity) in pp collisions [21, 23, 60]. A steeper increase is observed for J/ψ production at midrapidity [22, 24]. All models for J/ψ production in pp collisions at midrapidity (PYTHIA 8.2, model with coherent particle production (CPP) [61], EPOS3 [62], Color Glass Condensate effective theory (CGC) [63], 3-pomeron CGC [64], and percolation [54]) predict a faster-than-linear increase of the yields with charged-particle

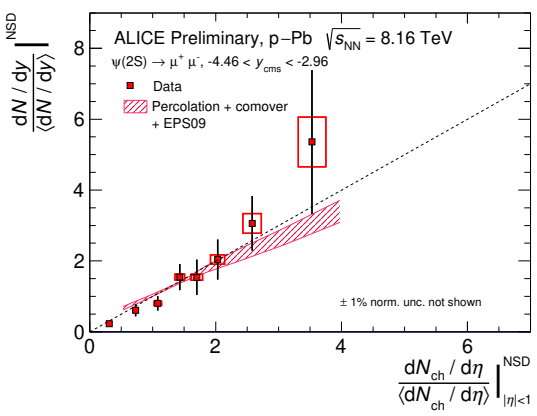

(a) Normalized $\psi(2S)$ yield

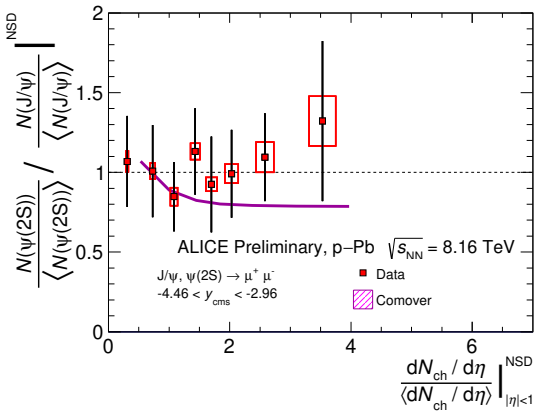

(b) Normalized ratio of $\psi(2S)$ over J/ψ

Fig. 5: The normalized $\psi(2S)$ yield and the ratio of normalized $\psi(2S)$-over-J/ψ yields at $-4.46 < y_{cms} < -2.96$ as a function of the normalized charged-particle pseudorapidity density in p–Pb collisions at $\sqrt{s_{NN}} = 8.16$ TeV. Measurements are compared with the percolation calculation [53] coupled with comover model [5] and EPS09 nPDF [58]. Quoted is the correlated event-class normalization uncertainty.

pseudorapidity density at midrapidity [22]. This is the consequence of a relative reduction of the charged-particle multiplicity at high multiplicities due to different physics mechanisms (color reconnection, coherent particle production, 3-gluon fusion, saturation, or percolation). The percolation model slightly overestimates the yield at high multiplicity, while PYTHIA 8.2 and EPOS3 underpredict the data. The CPP, CGC, and 3-pomeron CGC models give a good description of the measurements. To interpret these results, one should keep in mind that in all models, except PYTHIA, only the prompt component is considered, and the non-prompt contribution exhibits a stronger increase than the prompt one with multiplicity in PYTHIA 8.2 [22]. Model calculations predict a slightly smaller increase for J/ψ yields at large rapidity than at midrapidity with respect to charged-particle pseudorapidity density at midrapidity, consistent with the measurements. This suggests that the influence of the physics mechanisms at play differs for large and midrapidity J/ψ. The measurements presented in this Note for $\psi(2S)$ and in Ref. [60] for bottomonium ground and excited states at large rapidity are in agreement with this picture. It should be noted that, despite the recent progress, there are not many predictions available for excited charmonium states or bottomonium states as a function of charged-particle multiplicity.

6 Summary

The first measurements of $\psi(2S)$ production and of the $\psi(2S)$-over-J/ψ production ratio as a function of charged-particle multiplicity in pp and p–Pb collisions at the LHC are presented. Charmonium yields were measured at large rapidity, whereas charged-particle multiplicity was measured at central rapidity. Both charmonium yields and the charged-particle multiplicity have been normalized to their respective multiplicity-integrated values. The normalized $\psi(2S)$ yield increases with the normalized charged-particle density in both collision systems with an approximately linear trend with slope close to unity. The normalized $\psi(2S)$-over-J/ψ yield ratio is compatible with unity independently of the charged-particle multiplicity within uncertainties, suggesting a similar multiplicity dependence for excited and ground state charmonium states. The results can be described by models (PYTHIA 8.2 , percolation + comover + EPS09).

The measurements of the charged-particle multiplicity dependence of excited-to-ground state ratios provide additional constraints to models. The results for charmonium and bottomonium states at large rapidity in pp and p–Pb collisions provide a coherent picture, with ratios compatible with unity. The precision of the measurements does not allow one to rule out neither the decrease with increasing charged-particle

multiplicity predicted by the comover model, nor the nearly flat trend of PYTHIA 8.2 calculations. Bottomonium excited-to-ground state ratios at midrapidity show a smooth decreasing trend with increasing charged-particle pseudorapidity density at midrapidity from pp to p–Pb and to Pb–Pb collisions [65, 66]. A data-to-model comparison is unfortunately missing for the latter.

The forthcoming higher luminosity data taking at the LHC will allow one to improve the precision of the measurement and to perform more differential studies, bringing further inputs to clarify the picture.

References

[1] G. T. Bodwin, E. Braaten, and G. P. Lepage, "Rigorous QCD analysis of inclusive annihilation and production of heavy quarkonium", *Phys. Rev. D* **51** (1995) 1125–1171, arXiv:hep-ph/9407339. [Erratum: Phys.Rev.D 55, 5853 (1997)].

[2] Y.-Q. Ma and R. Venugopalan, "Comprehensive Description of J/ψ Production in Proton-Proton Collisions at Collider Energies", *Phys. Rev. Lett.* **113** no. 19, (2014) 192301, arXiv:1408.4075 [hep-ph].

[3] R. Vogt, "Shadowing and absorption effects on J/ψ production in *dA* collisions", *Phys. Rev. C* **71** (May, 2005) 054902. https://link.aps.org/doi/10.1103/PhysRevC.71.054902.

[4] F. Arleo and S. Peigné, "Quarkonium suppression in heavy-ion collisions from coherent energy loss in cold nuclear matter", *JHEP* **10** (2014) 073, arXiv:1407.5054 [hep-ph].

[5] E. G. Ferreiro, "Excited charmonium suppression in proton–nucleus collisions as a consequence of comovers", *Phys. Lett. B* **749** (2015) 98–103, arXiv:1411.0549 [hep-ph].

[6] T. Matsui and H. Satz, "J/ψ Suppression by Quark-Gluon Plasma Formation", *Phys. Lett. B* **178** (1986) 416–422.

[7] **ALICE** Collaboration, S. Acharya *et al.*, "Centrality and transverse momentum dependence of inclusive J/ψ production at midrapidity in Pb–Pb collisions at $\sqrt{s_{\rm NN}}$ = 5.02 TeV", *Phys. Lett. B* **805** (2020) 135434, arXiv:1910.14404 [nucl-ex].

[8] **ALICE** Collaboration, S. Acharya *et al.*, "Inclusive J/ψ production at forward and backward rapidity in p-Pb collisions at $\sqrt{s_{\rm NN}}$ = 8.16 TeV", *JHEP* **07** (2018) 160, arXiv:1805.04381 [nucl-ex].

[9] **ALICE** Collaboration, S. Acharya *et al.*, "Prompt and non-prompt J/ψ production and nuclear modification at mid-rapidity in p–Pb collisions at $\sqrt{\mathbf{s}_{\rm NN}} = \mathbf{5.02}$ TeV", *Eur. Phys. J. C* **78** no. 6, (2018) 466, arXiv:1802.00765 [nucl-ex].

[10] **ALICE** Collaboration, S. Acharya *et al.*, "Υ production in p–Pb collisions at $\sqrt{s_{\rm NN}}$ = 8.16 TeV", *Phys. Lett. B* **806** (2020) 135486, arXiv:1910.14405 [nucl-ex].

[11] **LHCb** Collaboration, R. Aaij *et al.*, "Prompt and nonprompt J/ψ production and nuclear modification in p–Pb collisions at $\sqrt{s_{\rm NN}} = 8.16$ TeV", *Phys. Lett. B* **774** (2017) 159–178, arXiv:1706.07122 [hep-ex].

[12] **LHCb** Collaboration, R. Aaij *et al.*, "Study of Υ production in p–Pb collisions at $\sqrt{s_{\rm NN}} = 8.16$ TeV", *JHEP* **11** (2018) 194, arXiv:1810.07655 [hep-ex]. [Erratum: JHEP 02, 093 (2020)].

[13] **CMS** Collaboration, A. M. Sirunyan *et al.*, "Measurement of prompt and nonprompt J/ψ production in pp and pPb collisions at $\sqrt{s_{\rm NN}} = 5.02$ TeV", *Eur. Phys. J. C* **77** no. 4, (2017) 269, arXiv:1702.01462 [nucl-ex].

[14] **ALICE** Collaboration, S. Acharya *et al.*, "Measurement of nuclear effects on $\psi(2S)$ production in p-Pb collisions at $\sqrt{s_{NN}} = 8.16$ TeV", *JHEP* **07** (2020) 237, arXiv:2003.06053 [nucl-ex].

[15] **LHCb** Collaboration, R. Aaij *et al.*, "Study of $\psi(2S)$ production and cold nuclear matter effects in p–Pb collisions at $\sqrt{s_{NN}} = 5$ TeV", *JHEP* **03** (2016) 133, arXiv:1601.07878 [nucl-ex].

[16] **ALICE** Collaboration, J. Adam *et al.*, "Centrality dependence of inclusive J/ψ production in p-Pb collisions at $\sqrt{s_{NN}} = 5.02$ TeV", *JHEP* **11** (2015) 127, arXiv:1506.08808 [nucl-ex].

[17] **ALICE** Collaboration, J. Adam *et al.*, "Centrality dependence of ψ(2S) suppression in p-Pb collisions at $\sqrt{s_{NN}}$ = 5.02 TeV", *JHEP* **06** (2016) 050, arXiv:1603.02816 [nucl-ex].

[18] **ALICE** Collaboration, D. Adamová *et al.*, "J/ψ production as a function of charged-particle pseudorapidity density in p-Pb collisions at $\sqrt{s_{NN}} = 5.02$ TeV", *Phys. Lett. B* **776** (2018) 91–104, arXiv:1704.00274 [nucl-ex].

[19] **ALICE** Collaboration, S. Acharya *et al.*, "Centrality dependence of J/ψ and ψ(2S) production and nuclear modification in p-Pb collisions at $\sqrt{s_{NN}} = 8.16$ TeV", *JHEP* **02** (2021) 002, arXiv:2008.04806 [nucl-ex].

[20] **ALICE** Collaboration, B. Abelev *et al.*, "J/ψ Production as a Function of Charged Particle Multiplicity in pp Collisions at $\sqrt{s} = 7$ TeV", *Phys. Lett. B* **712** (2012) 165–175, arXiv:1202.2816 [hep-ex].

[21] **ALICE** Collaboration, S. Acharya *et al.*, "Forward rapidity J/ψ production as a function of charged-particle multiplicity in pp collisions at $\sqrt{s} = 5.02$ and 13 TeV", arXiv:2112.09433 [nucl-ex].

[22] **ALICE** Collaboration, S. Acharya *et al.*, "Multiplicity dependence of J/ψ production at midrapidity in pp collisions at $\sqrt{s}$ = 13 TeV", *Phys. Lett. B* **810** (2020) 135758, arXiv:2005.11123 [nucl-ex].

[23] **ALICE** Collaboration, S. Acharya *et al.*, "J/ψ production as a function of charged-particle multiplicity in p-Pb collisions at $\sqrt{s_{NN}} = 8.16$ TeV", *JHEP* **09** (2020) 162, arXiv:2004.12673 [nucl-ex].

[24] **ALICE** Collaboration, J. Adam *et al.*, "Measurement of charm and beauty production at central rapidity versus charged-particle multiplicity in proton-proton collisions at $\sqrt{s} = 7$ TeV", *JHEP* **09** (2015) 148, arXiv:1505.00664 [nucl-ex].

[25] **ALICE** Collaboration, S. Acharya *et al.*, "Elliptic Flow of Electrons from Beauty-Hadron Decays in Pb-Pb Collisions at $\sqrt{s_{NN}}$ = 5.02 TeV", *Phys. Rev. Lett.* **126** no. 16, (2021) 162001, arXiv:2005.11130 [nucl-ex].

[26] **CMS** Collaboration, V. Khachatryan *et al.*, "Observation of Long-Range Near-Side Angular Correlations in Proton-Proton Collisions at the LHC", *JHEP* **09** (2010) 091, arXiv:1009.4122 [hep-ex].

[27] **ALICE** Collaboration, B. Abelev *et al.*, "Long-range angular correlations on the near and away side in *p*-Pb collisions at $\sqrt{s_{NN}} = 5.02$ TeV", *Phys. Lett. B* **719** (2013) 29–41, arXiv:1212.2001 [nucl-ex].

[28] **ATLAS** Collaboration, G. Aad *et al.*, "Observation of Associated Near-Side and Away-Side Long-Range Correlations in $\sqrt{s_{NN}}$ = 5.02 TeV Proton-Lead Collisions with the ATLAS Detector", *Phys. Rev. Lett.* **110** no. 18, (2013) 182302, arXiv:1212.5198 [hep-ex].

[29] **LHCb** Collaboration, R. Aaij *et al.*, "Measurements of long-range near-side angular correlations in $\sqrt{s_{\rm NN}} = 5$ TeV proton-lead collisions in the forward region", *Phys. Lett. B* **762** (2016) 473–483, arXiv:1512.00439 [nucl-ex].

[30] **CMS** Collaboration, V. Khachatryan *et al.*, "Evidence for collectivity in pp collisions at the LHC", *Phys. Lett. B* **765** (2017) 193–220, arXiv:1606.06198 [nucl-ex].

[31] **ALICE** Collaboration, S. Acharya *et al.*, "Search for collectivity with azimuthal J/ψ-hadron correlations in high multiplicity p-Pb collisions at $\sqrt{s_{\rm NN}}$ = 5.02 and 8.16 TeV", *Phys. Lett. B* **780** (2018) 7–20, arXiv:1709.06807 [nucl-ex].

[32] **CMS** Collaboration, A. M. Sirunyan *et al.*, "Elliptic flow of charm and strange hadrons in high-multiplicity p–Pb collisions at $\sqrt{s_{\rm NN}} = 8.16$ TeV", *Phys. Rev. Lett.* **121** no. 8, (2018) 082301, arXiv:1804.09767 [hep-ex].

[33] **CMS** Collaboration, A. M. Sirunyan *et al.*, "Observation of prompt J/ψ meson elliptic flow in high-multiplicity p–Pb collisions at $\sqrt{s_{\rm NN}} = 8.16$ TeV", *Phys. Lett. B* **791** (2019) 172–194, arXiv:1810.01473 [hep-ex].

[34] **ALICE** Collaboration, K. Aamodt *et al.*, "The ALICE experiment at the CERN LHC", *JINST* **3** (2008) S08002.

[35] **ALICE** Collaboration, B. B. Abelev *et al.*, "Performance of the ALICE Experiment at the CERN LHC", *Int. J. Mod. Phys. A* **29** (2014) 1430044, arXiv:1402.4476 [nucl-ex].

[36] **ALICE** Collaboration, B. B. Abelev *et al.*, "Centrality, rapidity and transverse momentum dependence of J/ψ suppression in Pb–Pb collisions at $\sqrt{s_{\rm NN}}$ = 2.76 TeV", *Phys. Lett. B* **734** (2014) 314–327, arXiv:1311.0214 [nucl-ex].

[37] **ALICE** Collaboration, K. Aamodt *et al.*, "Alignment of the ALICE Inner Tracking System with cosmic-ray tracks", *JINST* **5** (2010) P03003, arXiv:1001.0502 [physics.ins-det].

[38] **ALICE** Collaboration, E. Abbas *et al.*, "Performance of the ALICE VZERO system", *JINST* **8** (2013) P10016, arXiv:1306.3130 [nucl-ex].

[39] **ALICE** Collaboration, M. B. et al., "ALICE T0 detector", *IEEE Trans. Nucl. Sci.* **52** (2005) 1705–1711.

[40] **ALICE** Collaboration, "ALICE luminosity determination for pp collisions at $\sqrt{s} = 13$ TeV",.

[41] **ALICE** Collaboration, "ALICE luminosity determination for p-Pb collisions at $\sqrt{s_{\rm NN}} = 8.16$ TeV",.

[42] S. Roesler, R. Engel, and J. Ranft, "The Monte Carlo event generator DPMJET-III", in *International Conference on Advanced Monte Carlo for Radiation Physics, Particle Transport Simulation and Applications (MC 2000)*, pp. 1033–1038. 12, 2000. arXiv:hep-ph/0012252.

[43] T. Sjöstrand, S. Ask, J. R. Christiansen, R. Corke, N. Desai, P. Ilten, S. Mrenna, S. Prestel, C. O. Rasmussen, and P. Z. Skands, "An introduction to PYTHIA 8.2", *Comput. Phys. Commun.* **191** (2015) 159–177, arXiv:1410.3012 [hep-ph].

[44] R. Brun, F. Bruyant, F. Carminati, S. Giani, M. Maire, A. McPherson, G. Patrick, and L. Urban, "GEANT Detector Description and Simulation Tool",.

[45] T. Pierog, I. Karpenko, J. M. Katzy, E. Yatsenko, and K. Werner, "EPOS LHC: Test of collective hadronization with data measured at the CERN Large Hadron Collider", *Phys. Rev. C* **92** no. 3, (2015) 034906, arXiv:1306.0121 [hep-ph].

[46] **ALICE** Collaboration, S. Acharya *et al.*, "Charged-particle pseudorapidity density at mid-rapidity in p-Pb collisions at $\sqrt{s_{\rm NN}}$ = 8.16 TeV", *Eur. Phys. J. C* **79** no. 4, (2019) 307, arXiv:1812.01312 [nucl-ex].

[47] **ALICE** Collaboration, S. Acharya *et al.*, "Pseudorapidity distributions of charged particles as a function of mid- and forward rapidity multiplicities in pp collisions at $\sqrt{s}$ = 5.02, 7 and 13 TeV", *Eur. Phys. J. C* **81** no. 7, (2021) 630, arXiv:2009.09434 [nucl-ex].

[48] **ALICE** Collaboration, "Quarkonium signal extraction in ALICE",. https://cds.cern.ch/record/2060096.

[49] R. Shahoyan, *J/ψ and ψ(2S) production in 450 GeV pA interactions and its dependence on the rapidity and x_F*. PhD thesis, Lisboa U., 2001.

[50] **ALICE** Collaboration, J. Adam *et al.*, "Inclusive quarkonium production at forward rapidity in pp collisions at $\sqrt{s} = 8$ TeV", *Eur. Phys. J. C* **76** no. 4, (2016) 184, arXiv:1509.08258 [hep-ex].

[51] **Particle Data Group** Collaboration, P. A. Zyla *et al.*, "Review of Particle Physics", *PTEP* **2020** no. 8, (2020) 083C01.

[52] **ALICE** Collaboration, S. Acharya *et al.*, "Energy dependence of forward-rapidity J/ψ and ψ(2S) production in pp collisions at the LHC", *Eur. Phys. J. C* **77** no. 6, (2017) 392, arXiv:1702.00557 [hep-ex].

[53] N. Armesto, M. A. Braun, E. G. Ferreiro, and C. Pajares, "Percolation approach to quark - gluon plasma and J/ψ suppression", *Phys. Rev. Lett.* **77** (1996) 3736–3738, arXiv:hep-ph/9607239.

[54] E. G. Ferreiro and C. Pajares, "High multiplicity pp events and J/ψ production at LHC", *Phys. Rev. C* **86** (2012) 034903, arXiv:1203.5936 [hep-ph].

[55] E. G. Ferreiro, F. Fleuret, J. P. Lansberg, and A. Rakotozafindrabe, "Cold nuclear matter effects on J/ψ production: Intrinsic and extrinsic transverse momentum effects", *Phys. Lett. B* **680** (2009) 50–55, arXiv:0809.4684 [hep-ph].

[56] D. Kharzeev, E. Levin, M. Nardi, and K. Tuchin, "Gluon saturation effects on J/ψ production in heavy ion collisions", *Phys. Rev. Lett.* **102** (2009) 152301, arXiv:0808.2954 [hep-ph].

[57] A. Esposito, E. G. Ferreiro, A. Pilloni, A. D. Polosa, and C. A. Salgado, "The nature of $X(3872)$ from high-multiplicity pp collisions", *Eur. Phys. J. C* **81** (2021) 669, arXiv:2006.15044 [hep-ph].

[58] K. J. Eskola, H. Paukkunen, and C. A. Salgado, "EPS09: A New Generation of NLO and LO Nuclear Parton Distribution Functions", *JHEP* **04** (2009) 065, arXiv:0902.4154 [hep-ph].

[59] N. Armesto, A. Capella, and E. G. Ferreiro, "Charmonium suppression in lead-lead collisions: Is there a break in the J/ψ cross-section?", *Phys. Rev. C* **59** (1999) 395–404, arXiv:hep-ph/9807258.

[60] **ALICE** Collaboration, ALICE authors, "Multiplicity dependence of Υ production at forward rapidity in pp collisions at $\sqrt{s} = 13$ TeV",. In preparation.

[61] B. Z. Kopeliovich, H. J. Pirner, I. K. Potashnikova, K. Reygers, and I. Schmidt, "J/ψ in high-multiplicity pp collisions: Lessons from pA collisions", *Phys. Rev. D* **88** no. 11, (2013) 116002, arXiv:1308.3638 [hep-ph].

[62] K. Werner, B. Guiot, I. Karpenko, and T. Pierog, "Analysing radial flow features in p-Pb and pp collisions at several TeV by studying identified particle production in EPOS3", *Phys. Rev. C* **89** no. 6, (2014) 064903, arXiv:1312.1233 [nucl-th].

[63] Y.-Q. Ma, P. Tribedy, R. Venugopalan, and K. Watanabe, "Event engineering studies for heavy flavor production and hadronization in high multiplicity hadron-hadron and hadron-nucleus collisions", *Phys. Rev. D* **98** no. 7, (2018) 074025, arXiv:1803.11093 [hep-ph].

[64] E. Levin, I. Schmidt, and M. Siddikov, "Multiplicity dependence of quarkonia production in the CGC approach", *Eur. Phys. J. C* **80** no. 6, (2020) 560, arXiv:1910.13579 [hep-ph].

[65] **CMS** Collaboration, S. Chatrchyan *et al.*, "Event activity dependence of Y(nS) production in $\sqrt{s_{\mathrm{NN}}}$ = 5.02 TeV p–Pb and $\sqrt{s}$ = 2.76 TeV pp collisions", *JHEP* **04** (2014) 103, arXiv:1312.6300 [nucl-ex].

[66] **CMS** Collaboration, A. M. Sirunyan *et al.*, "Investigation into the event-activity dependence of Υ(nS) relative production in proton-proton collisions at $\sqrt{s}$ = 7 TeV", *JHEP* **11** (2020) 001, arXiv:2007.04277 [hep-ex].